PCCP

Cite this: *Phys. Chem. Chem. Phys.*, 2011, **13**, 19165–19170

www.rsc.org/pccp

PAPER

Anisotropy in the interaction of ultracold dysprosium

Svetlana Kotochigova* and Alexander Petrov†

Received 13th April 2011, Accepted 4th July 2011
DOI: 10.1039/c1cp21175g

The nature of the interaction between ultracold atoms with a large orbital and spin angular momentum has attracted considerable attention. It was suggested that such interactions can lead to the realization of exotic states of highly correlated matter. Here, we report on a theoretical study of the competing anisotropic dispersion, magnetic dipole–dipole, and electric quadrupole–quadrupole forces between two dysprosium atoms. Each dysprosium atom has an orbital angular momentum of $L = 6$ and a magnetic moment of $\mu = 10\ \mu_B$. We show that the dispersion coefficients of the ground state adiabatic potentials lie between 1865 a.u. and 1890 a.u., creating a non-negligible anisotropy with a spread of 25 a.u. and that the electric quadrupole–quadrupole interaction is weak compared to the other interactions. We also find that for interatomic separations $R < 50a_0$ both the anisotropic dispersion and magnetic dipole–dipole potential are larger than the atomic Zeeman splittings for external magnetic fields of order 10 G to 100 G. At these separations the atomic angular momentum can be reoriented. We finish by describing two scattering models for these inelastic m-changing collisions. A universal scattering theory is used to model loss due to the anisotropy in the dispersion and a Born approximation is used to model losses from the magnetic dipole–dipole interaction for the ^{164}Dy isotope. These models find loss rates that are of the same order of magnitude as the experimental value.

I. Introduction

In recent years significant effort has been devoted to the characterization of the interactions with submerged-shell 3d-transition-metal and 4f-rare-earth atoms.[1–8] These atoms have an electronic configuration with an unfilled inner shell shielded by a closed outer shell. They also tend to have a large magnetic moment due to a large number of unpaired electrons, which presents opportunities to explore the effect of anisotropic magnetic dipole–dipole interactions between them. Long-range dipolar interactions create conditions for realizing novel quantum states of highly correlated ultracold atomic matter.[7,9] This physics complements that proposed with ultracold polar molecules, another system in which exotic quantum phases are predicted.[10–13] Here, dipole–dipole forces originate from a non-zero electric dipole moment. Unlike for magnetic atoms, however, the electric dipole moment must be induced by an external electric field.

Submerged shell atoms are expected to have significantly suppressed inelastic, energy-releasing collisions because of shielding caused by the closed outer-shell electrons. This effect was first predicted and demonstrated for collisions between submerged-shell atoms with helium.[2–4,14] The suppression of inelastic loss with a He atom indicates that collisional anisotropy is small.

Recent measurements of the inelastic rates between two submerged-shell atoms, however, have seen no suppression and, in fact, the rate coefficients are of the same order of magnitude as for non-submerged shell atoms.[6,8,15,16] A possible explanation for these phenomena, given in ref. 8, is that most submerged-shell atoms have a non-zero orbital electron angular momentum L. This leads to a non-zero electrostatic quadrupole moment and anisotropic quadrupole–quadrupole interaction that, in principle, can cause substantial losses.

The concept of anisotropy in the interaction between two open-shell atoms in arbitrary angular momentum states was introduced in ref. 17 and the general ultracold energy dependence of spin depolarization transitions was discussed in ref. 18. Ref. 19 analyzes experimental measurements of ref. 2 and shows that electronic interaction anisotropy between open-shell lanthanide atoms and helium is extremely small. A similar conclusion was reached in ref. 20 for the interaction between magnetically-trapped Europium atoms. Their main mechanism for trap loss was found to be dipolar relaxation, whereas the hyperfine and spin–exchange interactions are negligible for the spin-polarized atoms.

In this paper we propose and discuss another mechanism that leads to losses. We will show that the large loss rate of the order 10^{-10} cm^3 s^{-1}, observed in ref. 6, 8 and 16, might have

Department of Physics, Temple University, Philadelphia, PA 19122-6082, USA. E-mail: skotoch@temple.edu
† Alternative address: St. Petersburg Nuclear Physics Institute, Gatchina, 188300; Department of Physics, St. Petersburg State University, 198904, Russia.

been due to anisotropy in the dispersion forces at short inter-atomic separations. This anisotropy is also induced by the nonzero L. We study this new mechanism of m-changing collisions for the submerged-shell atom with the largest magnetic moment, dysprosium. It has an unfilled $4f^{10}$ shell lying beneath a filled $6s^2$ shell leading to a large orbital, $L = 6$, and total, $j = 8$, angular momentum. Its ground $^5I_8$ state has a magnetic moment of $\mu = 10\ \mu_B$, where μ_B is the Bohr magneton. Only recently, the first laser cooling and trapping experiments of a large number of dysprosium atoms have been reported.[16] The first measurements of inelastic collisional rates in this study suggest that anisotropy in the inter-atomic forces plays a significant role.

The paper is organized as follows. We first analyze the isotropic and anisotropic dispersion interaction between two Dy atoms in Section II and compare it with the magnetic dipole–dipole and electrostatic quadrupole–quadrupole interactions. The dispersion coefficients are calculated from atomic transition frequencies and dipole moments. The quadrupole moment of Dy is determined from a multi-configuration electronic structure calculation. In Section III we study the relative strength of the interactions in the presence of an external magnetic field and rotation of the atom–atom pair with respect to the space-fixed coordinate axes. In Section IV we use these interactions to find the first estimates of the inelastic loss rates and compare with experimental results.

II. Relative strength of interaction forces between ground state Dy atoms

In our model dysprosium atoms are described in a relativistic approximation, where electron spin S is strongly coupled to the electron orbital angular momentum L, and only the total electron angular momentum j matters. That is L and S never decouple and only the projection m of j changes in the collision. For a pair of interacting atoms only the sum of the projections of j on the internuclear axis is conserved. This description differs from that for collisions of alkali-metal atoms, which are often non-relativistic and potentials are labeled by the total electron spin.

The theoretical calculation of the ground state Dy_2 potentials and their dispersion parameters is challenging due to the complexity of the spin structure of the ground-state $^5I_8$ Dy atom. For example, there are 81 gerade and 72 ungerade potentials that dissociate to the $^5I_8 + {}^5I_8$ limit. In spite of this complexity we have begun to calculate the van der Waals C_6 coefficients for two interacting Dy atoms.

For two colliding atoms we can define the angular momentum $\vec{J} = \vec{j}_1 + \vec{j}_2$, its projection M along the direction of the external magnetic field $\vec{B}$, and its projection Ω along the internuclear axis. For this relativistic molecule the adiabatic Born–Oppenheimer (BO) potentials are labeled by $\Omega_\sigma^\pm$, where $\sigma = g/u$ for gerade and ungerade states, respectively. Gerade (ungerade) symmetry corresponds to superpositions of even (odd) values of J. The superscript $\pm$ is only relevant for $\Omega = 0$ states. For each Ω there are $17 - |\Omega|$ adiabatic Born–Oppenheimer (BO) potentials combined.

A. Electrostatic dispersion interaction

We describe the dispersion interaction potential for two ground-state atoms in the state $|j_1m_1,j_2m_2\rangle$ using degenerate second-order perturbation theory similar to that given in ref. 21. The magnetic quantum numbers m_1 and m_2 are projections along the internuclear axis of the total atomic angular momenta $\vec{j}_1$ and $\vec{j}_2$ for the two atoms, respectively. Here $j_1 = j_2 = 8$. (In this section we break with convention and use roman symbols for atomic projection quantum numbers on the internuclear axis.) Matrix elements of the dispersion potentials are

$$\begin{aligned}\langle j_1m_1,j_2m_2|U_{\rm disp}|j_1m_1',j_2m_2'\rangle &= -\frac{C_6(m_1m_2,m_1'm_2')}{R^6}\\ &= \sum_{\substack{n_aj_am_a\\ n_bj_bm_b}} \frac{1}{(E_1+E_2)-(E_{n_aj_a}+E_{n_bj_b})}\\ &\quad\times\langle j_1m_1,j_2m_2|\hat{V}_{dd}|n_aj_am_a,n_bj_bm_b\rangle\\ &\quad\times\langle n_aj_am_a,n_bj_bm_b|\hat{V}_{dd}|j_1m_1',j_2m_2'\rangle,\end{aligned} \tag{1}$$

where the $C_6(m_1m_2,m_1'm_2')$ form a matrix of dispersion coefficients, R is the separation between the atoms, the sums are over all electronic states $|n_aj_am_a,n_bj_bm_b\rangle$ of atoms a and b excluding states with energies $E_{n_aj_a}$ and $E_{n_bj_b}$ equal to the ground state energies E_1 and E_2. The operator $\hat{V}_{dd}$ is the dipole–dipole interaction Hamiltonian[21]

$$\hat{V}_{dd}(\vec{R}) = \frac{1}{4\pi\varepsilon_0}\frac{(\vec{d}_1\vec{d}_2)-3d_{1z}d_{2z}}{R^3} \tag{2}$$

where ε_0 is the electric constant, $\vec{d}_1$ and $\vec{d}_2$ are the electric dipole operators for the two atoms, and d_{1z} and d_{2z} are their components along the internuclear axis.

Using the Wigner–Eckart theorem we write the matrix C_6 as

$$C_6(m_1m_2,m_1'm_2') = \sum_{j_aj_b} K_{j_aj_b}^{j_1j_2} A_{m_1m_2,m_1'm_2'}^{j_1j_2j_aj_b}, \tag{3}$$

where

$$\begin{aligned}A_{m_1m_2,m_1'm_2'}^{j_1j_2j_aj_b} &= \sum_{m_a,m_b}(1+\delta_{m_1,m_a})(1+\delta_{m_1',m_a})\\ &\quad\times\begin{pmatrix} j_1 & 1 & j_a\\ -m_1 & (m_1-m_a) & m_a\end{pmatrix}\begin{pmatrix} j_2 & 1 & j_b\\ -m_2 & (m_2-m_b) & m_b\end{pmatrix}\\ &\quad\times\begin{pmatrix} j_a & 1 & j_1\\ -m_a & (m_a-m_1') & m_1'\end{pmatrix}\begin{pmatrix} j_b & 1 & j_2\\ -m_b & (m_b-m_2') & m_2'\end{pmatrix},\end{aligned}$$

and

$$K_{j_aj_b}^{j_1j_2} = \left(\frac{1}{4\pi\varepsilon_0}\right)^2\sum_{n_a,n_b}\frac{|\langle j_1||d_1||n_aj_a\rangle\langle j_2||d_2||n_bj_b\rangle|^2}{(E_{n_aj_a}+E_{n_bj_b})-(E_1+E_2)}.$$

Note that the $A_{m_1m_2,m_1'm_2'}^{j_1j_2j_aj_b}$ conserve the molecular projection $\Omega = m_1 + m_2 = m_1' + m_2'$ and are independent of atomic transition frequencies and dipole moments. For this homonuclear molecule gerade/ungerade symmetry states are most conveniently constructed by transforming to states of total $\vec{J}$.

Table 1 The $K_{j_a j_b}^{j_1 j_2}$ matrix elements in atomic units for the dipole transitions from $j_1 = j_2 = 8$ to $j_a, j_b = 7$, 8, or 9 for two interacting Dy atoms

j_a/j_b	7	8	9
7	71528.597	81313.663	88173.833
8	81313.662	92438.922	100240.311
9	88173.833	100240.311	108705.654

That is to states $|(j_1 j_2) J\Omega\rangle$ and noting that even (odd) J states have gerade (ungerade) symmetry.

There are six independent $K_{j_a j_b}^{j_1 j_2}$ for two Dy $^5I_8$ atoms as the selection rules of the electric dipole operator require that $|j_1 - 1| \leq j_a \leq j_1 + 1$ and $|j_2 - 1| \leq j_b \leq j_2 + 1$. For homonuclear dimers the $K_{j_a j_b}^{j_1 j_2}$ is symmetric under interchange of j_a and j_b. We have determined $K_{j_a j_b}^{j_1 j_2}$ using 62 experimental transition frequencies and oscillator strengths from the ground to various excited states of the Dy atom.[22] Table 1 lists the values of $K_{j_a j_b}^{j_1 j_2}$.

The adiabatic dispersion potentials and, thus, the long-range of the Born–Oppenheimer potentials are found by diagonalizing the C_6 matrices for each $\Omega_{g/u}^{\pm}$. Fig. 1 shows the adiabatic gerade and ungerade C_6 coefficients as a function of the projection quantum number Ω of the total angular momentum J on the interatomic axis. The number of adiabatic C_6 values is smaller for larger Ω. In fact, for $\Omega = 16$ there is only one potential. It has gerade symmetry. In total there are 81/72 dispersion coefficients corresponding to the ground state gerade/ungerade potentials. The coefficients in Fig. 1 show a smooth nearly parabolic behavior with the projection number Ω, even though the second-order perturbation treatment of the van der Waals potential suggests terms with up to a quartic dependence. In any case this Ω dependence is a consequence of the anisotropic coupling of the open f-shell electrons of the two atoms. As a result the interaction energy depends on the relative orientation of the atoms.

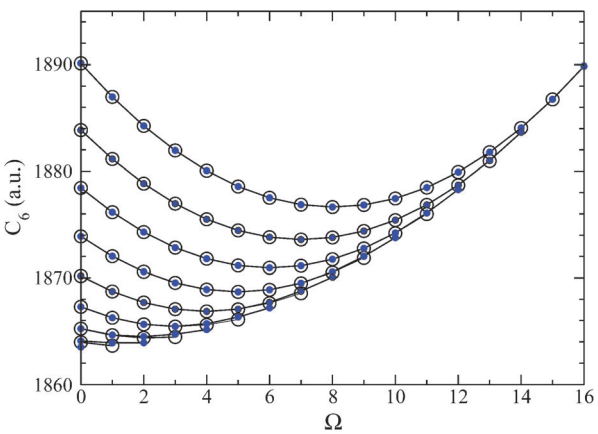

Fig. 1 Gerade (filled circles) and ungerade (open circles) adiabatic C_6 coefficients for the interaction between two ground $^5I_{j=8}$ state Dy atoms as a function of the projection Ω of the total angular momentum $\vec{j}$ on the interatomic axis. The difference between the dispersion coefficients for the gerade/ungerade symmetry is small and invisible on the graph. A larger C_6 coefficient implies a deeper Born–Oppenheimer potential.

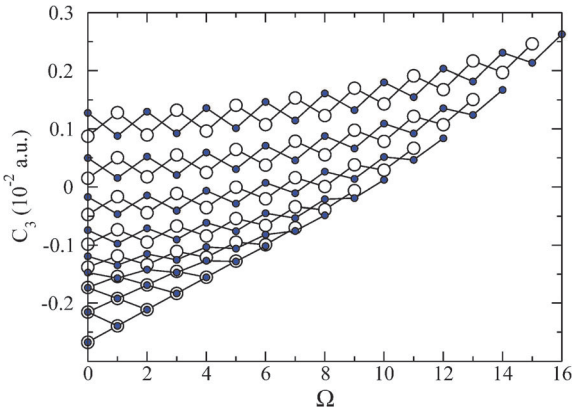

Fig. 2 Gerade (filled circles) and ungerade (open circles) adiabatic C_3 coefficients for the interaction between two ground $^5I_{j=8}$ state Dy atoms as a function of the projection Ω of the total angular momentum $\vec{j}$ on the interatomic axis. A larger C_3 coefficient implies a deeper Born–Oppenheimer potential.

B. Magnetic dipole–dipole and electrostatic quadrupole–quadrupole interaction

The matrix element of the magnetic dipole–dipole interaction between two magnetic dipoles $\vec{\mu} = g_j \mu_B \vec{j}$ is

$$\langle j_1 m_1, j_2 m_2 | U_{\mathrm{mdd}} | j_1 m_1', j_2 m_2' \rangle = -\frac{C_3(m_1 m_2, m_1' m_2')}{R^3} = \langle j_1 m_1, j_2 m_2 | \hat{V}_{\mu\mu} | j_1 m_1', j_2 m_2' \rangle, \quad (4)$$

where $\hat{V}_{\mu\mu}$ is the magnetic dipole–dipole operator

$$\hat{V}_{\mu\mu} = \frac{\mu_0 (g_j \mu_B)^2}{4\pi} \frac{(\vec{j}_1 \cdot \vec{j}_2) - 3 j_{1z} j_{2z}}{R^3}, \quad (5)$$

and $g_j = 1.24159$ is the g-factor for the ground $^5I_8$ state of the Dy atom,[23] and μ_0 is the magnetic constant. A more accurate value for the magnetic moment of Dy is $\mu = g_j \mu_B \times j = 9.93\ \mu_B$.

Fig. 2 shows the adiabatic gerade and ungerade C_3 coefficients as a function of Ω. These coefficients are obtained by diagonalizing the matrix, eqn (4). The values are both positive and negative. A comparison with the adiabatic C_6 coefficients in Fig. 1 shows a different Ω dependence.

A more accurate description of the long-range interaction is obtained by first adding the dispersion U_{disp} and magnetic dipole–dipole U_{mdd} interactions together and diagonalizing at each internuclear separation R. Unlike, for the previous cases the eigenfunctions now depend on R. As an example, the resulting adiabatic gerade potentials for projection $\Omega = 0$ as a function of R are shown in Fig. 3. At small R the dispersion interaction dominates, whereas for $R > 150 a_0$ the magnetic dipole–dipole interaction plays a major role. For intermediate R these forces compete leading to both attractive and repulsive potentials depending on the sign of the C_3 coefficient.

Our unrestricted coupled cluster calculation with single, double, and perturbative triple excitations UCCSD(T)[24] shows that the quadrupole moment of the Dy atom in the $^5I_8$ state is very small and equal to $Q = -0.00524$ a.u., defined as the mean value of the spherical quadrupole operator[25] for the stretched state $j = m = 8$. As a result the quadrupole–quadrupole

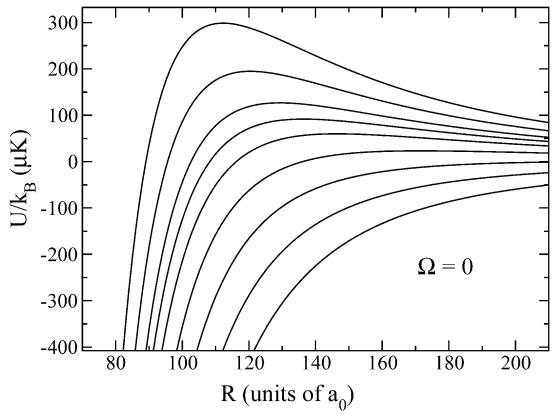

Fig. 3 Adiabatic gerade interaction potentials of the combined electrostatic dispersion and magnetic dipole–dipole forces between two Dy atoms in the ground $^5I_8$ state and projection $\Omega = 0$. Here k_B is the Boltzmann constant. The effect of rotation is not included.

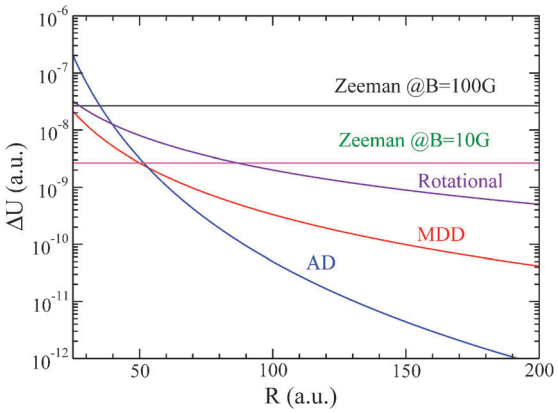

Fig. 4 Level splitting due to the dominant interaction forces in atomic units as a function of interatomic separation. In atomic units the Zeeman splitting is $g_jB/2$, the splitting between $\ell = 0$ and 2 rotational levels is given by $6/(2m_rR^2)$, the splitting due to the magnetic dipole–dipole (MDD) interaction is $2\alpha^2 j(g_j/2)^2/R^3$, where α is the fine structure constant, and the anisotropic dispersion (AD) interaction is $\Delta C_6/R^6$, where $\Delta C_6 = 25$ a.u. Here m_r is the reduced mass in units of the electron mass.

interaction energy is seven orders of magnitude weaker than the other atom–atom interactions. A much simpler Hartree–Fock calculation gives $Q \approx -0.1$ a.u. indicating that correlation effects are important reducing the quadrupole moment by an order of magnitude.

III. Interactions in a magnetic trap

We now analyze the relative strength of all interactions between two Dy atoms in a magnetic field. The magnetic field is added as either the atoms are held in a magnetic trap[16] with a spatially varying field strength or are held in an optical trap with a homogeneous B field to control the interaction between the atoms. In addition, the molecule can rotate, which is described by the Hamiltonian $\hbar^2\vec{\ell}^2/(2m_rR^2)$, where $\vec{\ell}$ is the relative orbital angular momentum between the two atoms and m_r is the reduced mass.

It is convenient to choose a coordinate system with projection quantum numbers defined along the external magnetic field direction. Again following convention, projection quantum numbers are labeled by roman symbols. In this coordinate system the rotational and Zeeman interactions as well as the isotropic or "average" dispersion potential shift molecular levels and cannot cause inelastic transitions, whereas the magnetic dipole–dipole interaction and the anisotropic component of the dispersion potential lead to coupling between different rotational and Zeeman components. As a result to first order, the angular momentum projection M of $\vec{J}$ can change up to 2 units due to the magnetic dipole interaction and up to 4 units due to the anisotropic dispersion potential.[26]

Fig. 4 shows various anisotropic properties that can lead to reorientation of the Dy angular momenta as a function of R. Firstly, the Zeeman splitting $g_j\mu_BB$ between neighboring magnetic sublevels for the magnetic field strength of 10 and 100 Gauss is shown. The anisotropic potential $\Delta C_6/R^6$ is drawn assuming a typical value of $\Delta C_6 = 25$ a.u., based on the spread of the C_6 value shown in Fig. 1. We also present the splitting between the rotational levels $\ell = 0$ and 2 of the ground state as $6\hbar^2/(2m_rR^2)$. Finally, the value of splitting due to magnetic dipole–dipole interaction is given.

For different interatomic separations different forces dominate. In fact, when the curves for the magnetic dipole or anisotropic dispersion interaction cross the Zeeman or rotational energies m-changing collisions can occur. At large R the Zeeman splitting dominates. Both magnetic dipole–dipole and anisotropic electrostatic curves cross the Zeeman $B = 100$ G curve at $R < 35a_0$, where chemical bonding should play an important role as well. For the weaker magnetic field of $B = 10$ G the angular momentum coupling occurs for R near $50a_0$. The interactions will lead to mixing of rotational levels for $R < 50a_0$ as well.

IV. First estimate of inelastic rate coefficients

In this paper we complete our analysis of the interaction between ultracold bosonic ^{164}Dy atoms by a first estimate of inelastic loss rates due to the anisotropy in the dispersion and magnetic dipole–dipole interaction. We will perform a separate estimate of losses from these interactions. For both cases we consider atoms in a magnetic field with a strength of the order of 10 G as described in the recent experiment,[16] with the goal to model its losses. The experiment started from a gas of Dy atoms in a quadrupole magnetic trap with atoms distributed over atomic magnetic sublevels with a positive magnetic moment, *i.e.* states $|jm\rangle$ with $m > 0$ where the projection m is defined along the magnetic field direction. Inelastic m-changing collisions to states with $m \leq 0$ lead to atom loss.

We first describe a model for the loss due to the anisotropic dispersion potentials based on a universal single-channel scattering model developed and used in ref. 27–29. This universal loss model assumes scattering from a single potential of the form $-C_6/R^6 + \hbar^2\ell(\ell+1)/(2m_rR^2)$ for $R > R_c$ and that all flux that reaches the critical separation R_c undergoes irreversible m-changing collisions independent of scattering energy and partial wave $\vec{\ell}$.

For Dy we can use this universal model under several assumptions. We first note that the anisotropy ΔC_6 of the dispersion potential is small compared to the average or isotropic dispersion potential. Secondly, an external magnetic

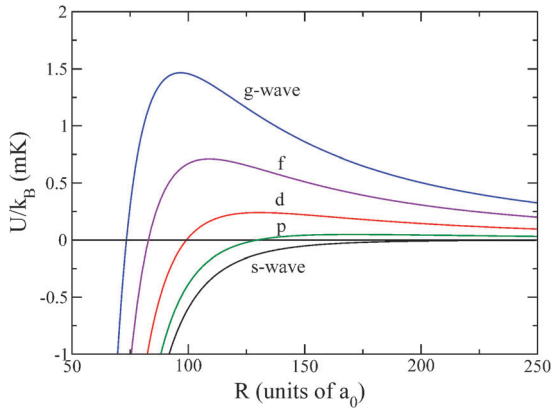

Fig. 5 Dispersion interaction potentials for $C_6 = 1890$ a.u. for the lowest five partial waves with centrifugal barriers for *p*-, *d*-, *f*-, and *g*-waves.

field is applied that splits the different m levels and, as shown in Fig. 4, the m-sublevel changes occur between $R_c = 35a_0$ and $50a_0$ depending on the magnetic field strength. We can therefore apply the universal model assuming a mean isotropic C_6 value and that, due to the anisotropic dispersion potential, no flux returns from $R < R_c$.

For temperatures between 100 μK to 1 mK only a few partial waves ℓ contribute to the collisions. Fig. 5 illustrates this by showing the centrifugal barriers for p, d, f and g partial waves as a function of R. The temperature range of interest lies well below the g-wave barrier. Within the universal scattering model the contribution to the inelastic rate coefficient for partial wave ℓ and projection m_ℓ is

$$K_{\ell m_\ell}(E) = v_i \frac{\pi}{k_i^2}(1 - |S_{\ell m_\ell}(E)|^2), \qquad (6)$$

where $E = k_i^2/(2m_r)$ is the collision energy, k_i is the initial relative wavenumber, v_i is the initial relative velocity, and $S_{\ell m_\ell}(E)$ are diagonal scattering S-matrix elements. The solution $\Psi_{\ell m_\ell}(R)$ of the radial Schrödinger equation for the single-channel potential with the boundary condition

$$\Psi_{\ell m_\ell}(R) \propto e^{-i(R_x/R)^2/2}$$

at a short range $R < R_c$ with $R_x = \sqrt[4]{2m_r C_6/\hbar^2}$ and

$$\Psi_{\ell m_\ell}(R) = \frac{e^{-ik_i R}}{\sqrt{k_i}} - S_{\ell m_\ell}(E)\frac{e^{ik_i R}}{\sqrt{k_i}}$$

at large R determines the elastic $S_{\ell m_\ell}$ matrix elements. The partial and total loss rate coefficients are $\beta_\ell(E) = 2\sum_{m_\ell} K_{\ell m_\ell}(E)$ and $\beta(E) = 2\sum_{\ell m_\ell} K_{\ell m_\ell}(E)$, respectively. The factor 2 is due to the fact that after each collision two atoms are lost. Partial and total inelastic loss rate coefficients for non-spin-polarized Dy atoms are shown in Fig. 6a for collision energies up to 1.5 mK. Both even and odd partial waves contribute to the losses. The figure shows that the loss rate for the different partial waves becomes large for collision energies approaching the corresponding centrifugal barrier. Moreover, except for extremely small collision energies the total loss rate coefficient slowly increases with energy. For comparison we have also indicated the unitarity limit for each partial wave. The unitary limit occurs when $|S_{\ell m_\ell}(E)|^2 = 0$ for

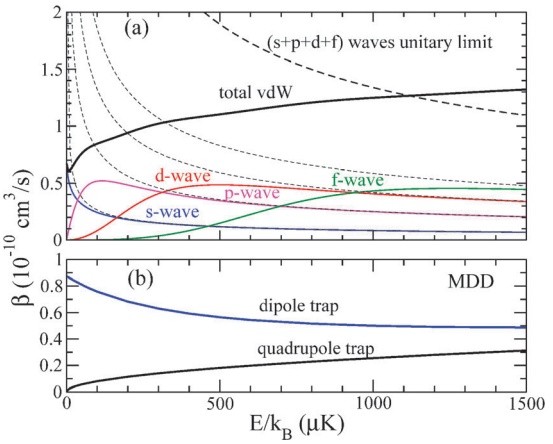

Fig. 6 The inelastic loss rate coefficient for a non-spin-polarized sample of ground state ^{164}Dy atoms as a function of collision energy based on a universal scattering model for losses due to the anisotropy of the dispersion potential (panel a) and a Born approximation for losses from the magnetic dipole–dipole interaction (panel b). For the universal scattering model rate coefficients for the lowest four partial waves as well as the summed rate are shown. The unitary limited loss rate coefficients for the lowest four partial waves are plotted as dashed lines. The loss rate coefficient for the magnetic dipole–dipole interaction is given for a quadrupole as well as a dipole trap with a constant magnetic field of $B = 10$ G.

all collision energies. At the unitary limit the cross-sections for elastic and inelastic scattering are equal. This is because elastic scattering is proportional to $|1 - S_{\ell m_\ell}(E)|^2$ and inelastic scattering necessarily implies the simultaneous presence of elastic scattering. The unitarity limit should not be confused with the unitarity of the S-matrix, containing both elastic and inelastic matrix elements.

We now turn to a model for losses due to inelastic m-changing collisions induced by the magnetic dipole–dipole interaction. For simplicity we assume that the atoms are in the stretched state with $m = +j$. We estimate this inelastic loss rate using first-order perturbation theory similar to that applied for the calculation of the dipolar relaxation rates in a gas of chromium atoms.[1] We immediately note that the magnetic moment of dysprosium or chromium atoms is large and, therefore, a perturbative theory may not provide an accurate loss rate. However, it is expected to give a reasonable estimate. Following ref. 1, the loss rate coefficient for a $M \to M - 1$ (*i.e.* from $M = 16$ to 15) collision, averaged over all possible relative orientations of the initial relative momentum $\vec{k}_i$, is

$$\gamma_1 = \frac{4\pi}{15} j^3 \left(\frac{\mu_0 (g_j \mu_B)^2 \mu_r}{2\pi\hbar^2}\right)^2 [1 + h(k_f/k_i)] \frac{\hbar k_f}{\mu_r}, \qquad (7)$$

where $\hbar_2 k_f^2/(2\mu_r) = \hbar_2 k_i^2/(2\mu_r) + g_j \mu_B B$ and

$h(x) = -1/2 - (3/4)(1 - x^2)^2 \log[x - 1/(x + 1)]/(x(1 + x^2))$

for $x > 1$.

Similarly, for a $M \to M - 2$ collision the rate coefficient is

$$\gamma_2 = \frac{2\pi}{15} j^2 \left(\frac{\mu_0 (g_j \mu_B)^2 \mu_r}{2\pi\hbar^2}\right)^2 [1 + h(k_f/k_i)] \frac{\hbar k_f}{\mu_r}, \qquad (8)$$

where now $\hbar^2k_f^2/(2\mu_r) = \hbar^2k_i^2/(2\mu_r) + 2g_j\mu_B B$. The total dipole–dipole loss rate is given by $\gamma = 2(\gamma_1 + \gamma_2)$ and shown as a function of collision energy in Fig. 6b for two trapping configurations, a quadrupole magnetic trap and a dipole trap with a constant magnetic field of $B = 10$ Gauss. In the quadrupole trap the magnetic field increases linearly from zero at the center of the trap. Consequently, colder atoms are exposed to smaller magnetic fields leading to smaller kinetic energy release. The losses from MDD go to zero near threshold in a quadrupole trap. In the dipole trap the loss rate approaches a constant value of $\beta = 0.87 \times 10^{-10}$ cm^3 s^{-1} near threshold. The factor 2 in the total loss rate γ indicates that after each collision two atoms are lost. However, in principle for shallow magnetic traps it is possible that only the $M \rightarrow M - 2$ collision leads to loss.

Ref. 16 measured a loss rate of $2.1(2) \times 10^{-10}$ cm^3 s^{-1} in a quadrupole magnetic trap for temperatures around 500 μK. The loss rates in Fig. 6 are smaller than the measured rate. One explanation is the presence of resonances in the scattering process. In fact, flux of atoms can return from small R, interfere with the incoming flux to lead to an increasing loss. We obtained a similar effect in our analysis of the reactive collisions between two KRb molecules.[30]

V. Conclusion

In conclusion, we have studied the origin of the anisotropy in the long-range interaction between ground state dysprosium atoms. This is a first step towards a complete multi-channel description of inelastic and elastic collisions between such atoms. We find van der Waals coefficients by using known atomic dipole moments and energy levels. Our coefficients form a lower bound. We show that the splitting between or anisotropy of the Born–Oppenheimer potentials is almost two orders of magnitude smaller than their average or isotropic potential. In addition, we have presented two approximate single-channel calculations to estimate inelastic losses when Dy atoms are not in the energetically-lowest Zeeman sublevel. The first model describes losses due to the anisotropy of the dispersion potentials and is based on a universal scattering theory. The second perturbative model describes losses due to the magnetic dipole–dipole interaction. The only way to obtain a clear and quantitative understanding of collisions between Dy atoms is by a coupled-channel calculation. We will do so in the near future. It will enable us to predict location of magnetic Feshbach resonances in the energetically-lowest Zeeman level.

Acknowledgements

This work is supported by grants of the Air Force Office of Scientific Research and NSF PHY-1005453. We acknowledge helpful discussions on the Dy electronic structure with Dr J. Reader and stimulating discussions with Dr B. Lev, Dr E. Tiesinga, and Dr J. Bohn.

References

1 S. Hensler, J. Werner, A. Griesmaier, P. O. Schmidt, A. Görlitz, T. Pfau, S. Giovanazzi and K. Rzazewski, *Appl. Phys. B: Lasers Opt.*, 2003, **77**, 765.
2 C. I. Hancox, S. C. Doret, M. T. Hummon, L. Luo and J. Doyle, *Nature*, 2004, **431**, 281.
3 C. I. Hancox, S. C. Doret, M. T. Hummon, R. V. Krems and J. M. Doyle, *Phys. Rev. Lett.*, 2005, **94**, 013201.
4 R. V. Krems, J. Klos, M. F. Rode, M. M. Szczesniak, G. Chalasiński and A. Dalgarno, *Phys. Rev. Lett.*, 2005, **94**, 013202.
5 J. Stuhler, A. Griesmaier, T. Koch, T. Pfau, S. Giovanazzi, P. Pedri and L. Santos, *Phys. Rev. Lett.*, 2005, **95**, 150406.
6 J. G. E. Harris, S. V. Nguyen, S. C. Doret, W. Ketterle and J. M. Doyle, *Phys. Rev. Lett.*, 2007, **99**, 223201.
7 T. Lahaye, T. Koch, B. Fröhlich, M. Fattori, J. Menz, A. Griesmaier, S. Giovanazzi and T. Pfau, *Nature*, 2007, **448**, 672.
8 C. B. Connolly, Y. Shan Au, S. C. Doret, W. Ketterle and J. M. Doyle, *Phys. Rev. A: At., Mol., Opt. Phys.*, 2010, **81**, 01000702.
9 B. Fregoso and E. Fradkin, *Phys. Rev. Lett.*, 2009, **103**, 205301; B. Fregoso and E. Fradkin, *Phys. Rev. B: Condens. Matter Mater. Phys.*, 2010, **81**, 214443.
10 R. Wilson, S. Ronen and J. Bohn, *Phys. Rev. A: At., Mol., Opt. Phys.*, 2009, **80**, 023614.
11 M. A. Baranov, A. Micheli, S. Ronen and P. Zoller, *Phys. Rev. A: At., Mol., Opt. Phys.*, 2011, **83**, 043602.
12 D.-W. Wang, M. D. Lukin and E. Demler, *Phys. Rev. Lett.*, 2006, **97**, 180413.
13 M. Lewenstein, *Nat. Phys.*, 2006, **2**, 309.
14 E. B. Aleksandrov, *et al.*, *Opt. Spektrosk.*, 1983, **54**, 1.
15 M.-J. Lu, V. Singh and J. D. Weinstein, *Phys. Rev. A: At., Mol., Opt. Phys.*, 2009, **79**, 050702.
16 M. Lu, S. Ho Youn and B. Lev, *Phys. Rev. Lett.*, 2010, **104**, 063001.
17 R. V. Krems, G. C. Groenenboom and A. Dalgarno, *J. Phys. Chem. A*, 2004, **108**, 8941.
18 R. V. Krems and A. Dalgarno, *Phys. Rev. A: At., Mol., Opt. Phys.*, 2003, **67**, 050704.
19 R. V. Krems and A. A. Buchachenko, *J. Chem. Phys.*, 2005, **123**, 101101.
20 Y. V. Suleimanov, *Phys. Rev. A: At., Mol., Opt. Phys.*, 2010, **81**, 022701.
21 A. J. Stone, *The theory of intermolecular forces*, Clarendon Press, London, 1996.
22 M. E. Wickliffe, J. E. Lawler and G. Nave, *J. Quant. Spectrosc. Radiat. Transfer*, 2000, **66**, 363–404; J. J. Curry, E. A. Den Hartog and J. E. Lawler, *J. Opt. Soc. Am. B*, 1997, **14**, 2788; V. N. Gorshkov, V. A. Komarovskii, A. L. Osherovich, N. P. Penkin and R. Khefferlin, *Opt. Spektrosk.*, 1980, **48**, 362.
23 Yu. Ralchenko, A. E. Kramida, J. Reader and NIST ASD Team (2010). NIST Atomic Spectra Database (ver. 4.0.1), http://physics.nist.gov/asd.
24 J. D. Watts, J. Gauss. and R. J. Bartlett, *J. Chem. Phys.*, 1993, **98**, 8718.
25 D. M. Brink and G. R. Satchler, *Angular Momentum*, 2nd edn, Oxford University Press, 1975.
26 R. Santra and C. H. Greene, *Phys. Rev. A: At., Mol., Opt. Phys.*, 2003, **67**, 062713.
27 P. S. Julienne and F. H. Mies, *J. Opt. Soc. Am. B*, 1989, **6**, 2257.
28 C. Orzel, M. Walhout, U. Sterr, P. S. Julienne and S. L. Rolston, *Phys. Rev. A: At., Mol., Opt. Phys.*, 1999, **59**, 1926.
29 E. R. Hudson, N. B. Gilfoy, S. Kotochigova, J. M. Sage and D. DeMille, *Phys. Rev. Lett.*, 2008, **100**, 203201.
30 S. Kotochigova, *New J. Phys.*, 2010, **12**, 073041.

